Effect of Austenite Grain Size on Acicular Ferrite Transformation in a HSLA Steel

Haitao Zhao[a, b]*, Eric J. Palmiere[a]

[a] The University of Sheffield, Department of Materials Science and Engineering, Sir

Robert Hadfield Building, Mappin Street, Sheffield S1 3JD, UK

[b] HBIS Group Technology Research Institute, HBIS Group, Shijiazhuang 050023, China

Corresponding author：H. Zhao

email：zhaohaitao@hbisco.com

Keywords: Austenite grain size; Acicular ferrite; Effective grain size; Bainitic ferrite; Austenite deformation

Abstract

Austenite grain size is well known to have a significant influence on various phase transformations in steels. Although the effects of many thermomechanical processing parameters on acicular ferrite (AF) transformation in HSLA steels have been investigated, little attention has been paid to the influence of austenite grain size. Therefore, in this research, different parameters of solid-solution heat treatment and rough deformation were adopted to generate austenite with different grain sizes and the effects of austenite grain size before deformation on the AF transformation and grain refinement were investigated. It was found that the reduction of prior-austenite grain size (PAGS) from 62.8μm to 37.0μm before austenite deformation promotes the AF transformation and simultaneously refines and homogenises the transformed

1

microstructures. A reciprocally increased density of deformation induced dislocations with the reduction of PAGS was proposed to account for these results, which not only increase the nucleation sites of AF but also suppress the lengthening of BF laths. Further reducing PAGS from 37.0μm to 22.3μm, the fraction of AF is not increased and the transformed microstructure is not refined. Possible differences in the type, distribution, and density of austenite deformation substructures between austenite with PAGSs of 37.0μm and 22.3μm were argued to be responsible for the cease of grain refinement. The relationship between effective grain sizes and the S_v parameter was investigated and an equation relating effective grain sizes with processing parameters was also proposed.

1. Introduction

High strength and high toughness are important requirements for high strength low alloy (HSLA) steels [1-3]. Following the steadily increased strength requirement for HSLA steels over the past 50 years, corresponding microstructures evolve from ferrite and pearlite to acicular ferrite (AF) and bainitic ferrite (BF) [4]. HSLA steels with an AF microstructure possess a better property combination (e.g., higher strength [5], better toughness [5], superior H_2S resistance [6], and better fatigue behaviour [7]) than those steels exhibiting a ferrite-pearlite microstructure. Additionally, the toughness of an AF microstructure is considerably higher than that of a BF microstructure [8].

The term acicular ferrite (AF) has been assigned to two different microstructures over the years, AF in steel welds [9-11] and AF in high strength low alloy (HSLA) steels

2

[7, 12, 13]. AF in steel welds actually is ferrite laths that nucleate heterogeneously on small non-metallic inclusions and grow in many different directions from these point nucleation sites [9, 10]. Based on extensive investigations [11, 14, 15], the transformation mechanism of AF in steel welds was found to be similar to that of bainite, except for the requirement of intragranular nucleation sites. Therefore, AF in steel welds has been known as intragranularly nucleated bainite [11].

While in HSLA steels, AF was defined by Smith et al. [12] in 1972 as "a highly substructured, non-equiaxed ferrite that forms upon continuous cooling by a mixed diffusion and shear mode of transformation that begins at a temperature slightly higher than the upper bainite transformation range". Although AF in HSLA steels nucleates intragranularly and its transformation mechanism is bainitic [16-18], the intragranular nucleation sites of AF in HSLA steels are dislocation substructures instead of non-metallic inclusions [8, 19-21]. This difference leads to distinct morphology characteristics of AF in HSLA steels which are small grain sizes, irregular grain shapes and a chaotic grain arrangement [7, 12, 13], in contrast to the radiating morphology of AF laths in steel welds [9-11].

To obtain an AF dominant microstructure in HSLA steels, the effects of various processing parameters, including austenite deformation below the recrystallisation-stop temperature ($T_{5\%}$) [13, 21, 22] and cooling rates [23-25], have been investigated. However, little attention has been paid to the influence of prior-austenite grain size (PAGS). PAGS is well known to have a significant influence on various phase transformations of steels [26-28]. With respect to AF in steel welds, it was found that

the decomposition of austenite is a competition between BF nucleated on austenite grain boundaries and AF nucleated intragranularly on non-metallic inclusions [29, 30]. By increasing PAGS, the fraction of intragranularly nucleated AF was increased, replacing the boundary nucleated BF, and this was attributed to the reduction of austenite grain boundary area and thus the nucleation site density of BF [29, 30].

Since AF in HSLA steels also nucleates intragranularly [8, 19-21], it is reasonable to assume that the fraction of AF will also be influenced by the change of PAGS. As proposed by the present authors [31], austenite deformation and proper cooling rates are prerequisites for the AF transformation in HSLA steels. Therefore, in this research specimens with various austenite grain sizes were developed and subjected to plane strain compressions and accelerated cooling to investigate the effect of PAGS before austenite deformation on the AF transformation in a HSLA steel [32].

2. Material and methods

The chemical composition of the tested steel is shown in Table 1. In order to fully dissolve the Nb-containing precipitates and shorten the preheating time during testing, all specimens were subjected to solid-solution heat treatments at 1250°C with argon atmosphere protection, and then were water quenched directly from 1250°C to room temperature.

Table 1 Chemical Compositions (wt%)

C	Mn	Si	S	P	Nb	Cr	Ni	Cu	Ti	N
0.045	1.43	0.14	<0.003	<0.01	0.09	0.21	0.12	0.21	0.01	0.0039

The processing route is illustrated in Figure 1. The heat-treated samples were reheated to 1200°C at a rate of 10°C/s, held for 2 minutes for equilibration, and then cooled at a rate of 5°C/s to 1100°C for a rough deformation with strain1 at a constant true strain rate of $10s^{-1}$. After that, the samples were cooled immediately to 950°C at a rate of 5°C/s for a finish deformation with strain2 of 0.5. This finish deformation was also performed at a constant true strain rate of $10s^{-1}$ and was followed by an accelerated cooling from 950°C to 500°C at a rate of 10°C/s, a slow cooling from 500°C to 350°C at a rate of 1°C/s, and finally a water quenching from 350°C to room temperature.
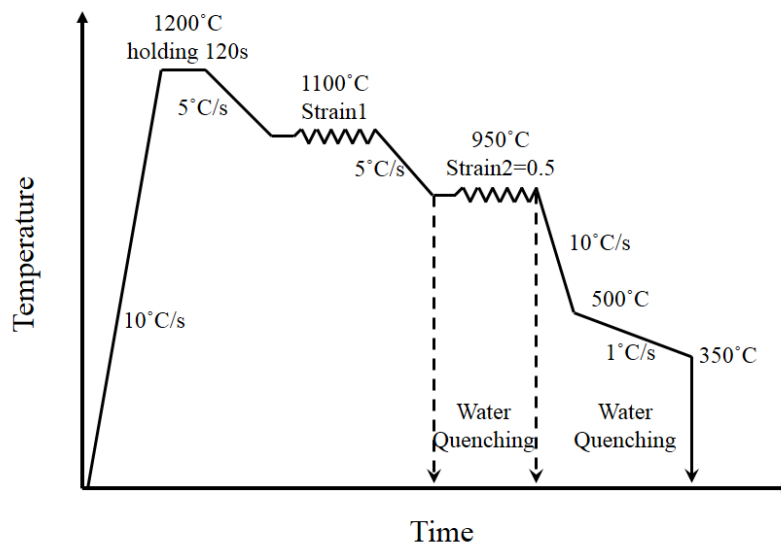
Figure 1 Schematic illustration of the thermomechanical testing profile.

During the solid-solution heat treatment and thermomechanical processing illustrated above, parameters of the solid-solution heat treatment, the reheating and the rough deformation (strain1) all can influence the PAGS before the finish deformation (strain2). However, attention must be paid to choosing the suitable parameters to generate different PAGSs, especially the reheating temperature and duration. During

5

reheating, not only the PAGS but also the dissolution status of Nb-containing precipitates are changed by altering the reheating temperatures or durations [33], which makes the investigation on the effect of PAGS biased. Differently, if the standard solid-solution heat treatment can dissolve most of the Nb-containing precipitates, prolonging the duration of the heat treatment can result in a larger PAGS without greatly changing the Nb-containing precipitates dissolution status. In addition, altering the rough deformation (strain1) also have little influence on the Nb-containing precipitates dissolution status simply due to the high temperature (1100˚C) of this deformation at which the precipitation of Nb carbide or carbonitride is very slow. Therefore, to generate austenite with different grain sizes, different combinations of solid solution heat treatment and rough deformation (strain 1) were used as shown in Table 2 [34] and S, M, L and XL were designated to the specimens with different PAGSs. Additionally, specimen S, M, L and XL were also water quenched directly from 950˚C before or after the finish deformation (strain2 of 0.5) to reveal the prior-austenite microstructures with different PAGSs.

Table 2 Heat treatment and austenite deformation parameters.

Specimen names	S	M	L	XL
Heat treatment temperature (˚C)	1250	1250	1250	1250
Heat treatment duration (s)	1800	1800	7200	7200
Strain1 volume	0.7	0.3	0.3	0
Prior-austenite grain size (μm)	22.3	37.0	52.4	62.8

Samples for metallographic observation were cut on the rolling direction (RD)–normal direction (ND) plane and prepared carefully. A 2% nital solution was used to show the transformed microstructure and a saturated aqueous picric acid solution was used to reveal the prior-austenite grain boundaries (PAGBs). PAGSs were measured optically by the linear intercept method. Optical microscopy (OM) and scanning electron microscopy (SEM) observations were carried out on Nikon Eclipse LV150 and FEI InspectF, respectively.

EBSD mappings were performed via a FEI Sirion electron microscope with a HKL Nordlys detector. Orientation maps with a step size of 0.2 μm and accelerating voltage of 20kV were obtained on the RD-ND plane for each sample. To reduce the mis-indexing of phases in this complex microstructure, α iron (BCC) was chosen as the only matching unit. Following a recommended method [35], noise points of raw data were removed and non-indexed points were filled with the common orientation of their neighbours using HKL Channel 5 Tango software.

3. Results

3.1 Prior-austenite microstructures

Optical micrographs of the prior-austenite grain boundaries (PAGBs) both before and after strain2 for specimen S, M, L and XL are shown in Figure 2. It is clear from Figure 2a~d that through adjusting the solid-solution heat treatment durations and the volumes of strain1, fully recrystallised austenite with different grain sizes were obtained before strain2. PAGS measurement results are shown in Table 2, varying from

22.3μm to 62.8μm. After the finish deformation (strain2 of 0.5), austenite grains of all specimens remain in a deformed state as shown in Figure 2e~h and there is no sign of the onset of dynamic recrystallization (DRX). This corresponds well with the result shown in research [36] that the austenite non-recrystallization temperature is 1060˚C for a HSLA steel with a similar chemical composition to the tested steel in this research but a slightly higher Nb content (0.1 wt%).
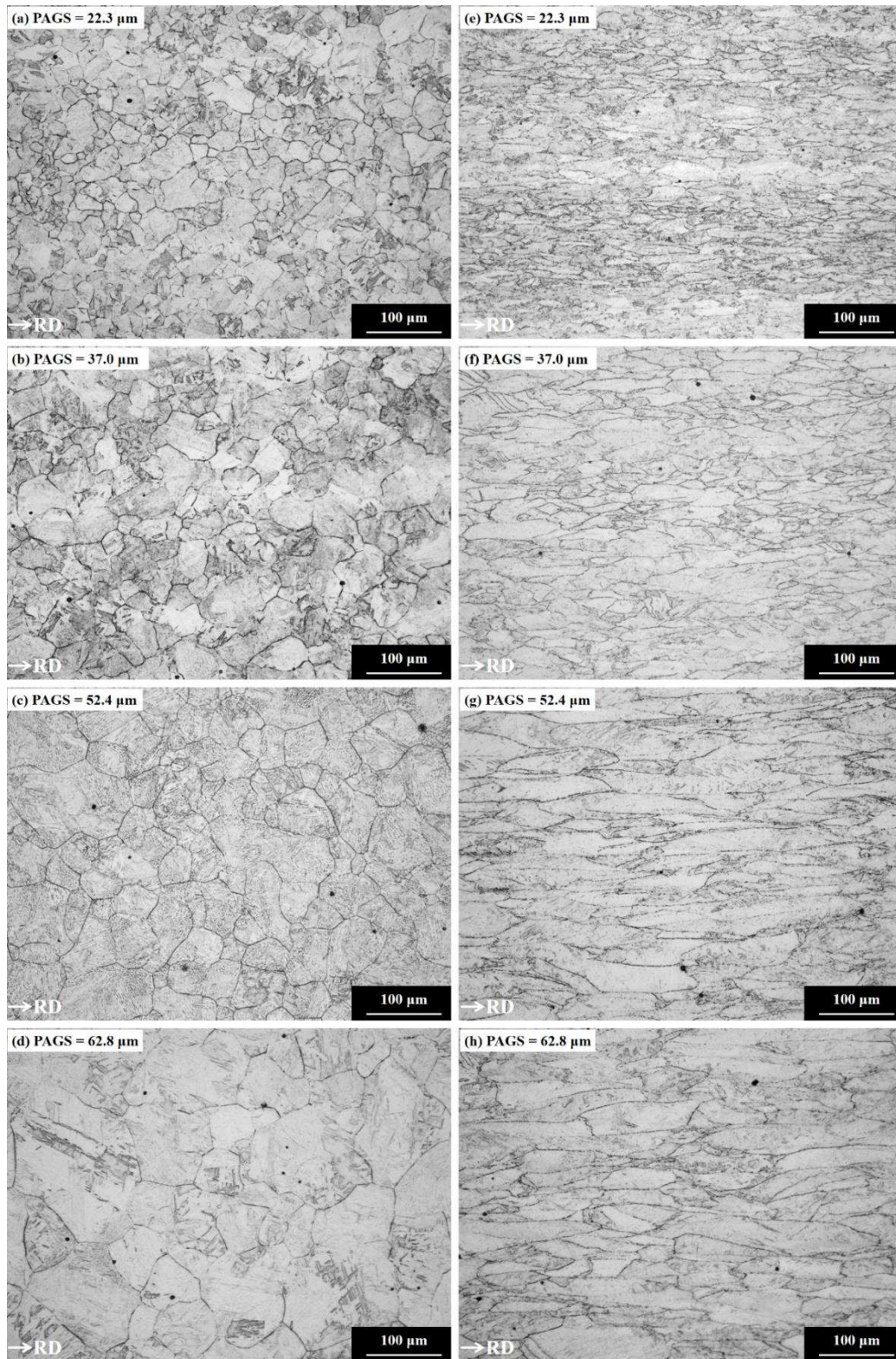
Figure 2 Optical micrographs of prior-austenite grain boundaries for specimen S, M, L and XL respectively: (a)~(d) before strain2 at 950˚C; (e)~(h) after strain2 of 0.5 at 950˚C.

3.2 Transformed microstructures

According to the classification systems proposed by Araki et al. [2] and Krauss et al. [3], ferritic transformation products can be divided into several categories including polygonal ferrite (PF), quasi-polygonal ferrite (QF), granular bainite (GB), acicular ferrite (AF) and lath bainite (LB). PF and QF are reconstructive transformation products. PF forms at the slowest cooling rates and the highest transformation temperatures. It nucleates at austenite grain boundaries and grows into an equiaxed shape [3]. QF often forms in very-low-carbon steels under rapid cooling [4]. In this condition, single-phase austenite can transform into single-phase ferrite without a composition change, and the QF grains formed are usually coarse and have irregular and jagged grain boundaries [3]. At lower transformation temperatures, AF, GB and LB transformations become dominant [5, 6]. The transformation and microstructural characteristics of AF are illustrated in the introduction section. GB usually forms at relatively high temperatures and mainly consists of wide parallel laths. The boundaries between GB laths are usually low angle grain boundaries (LAGBs) with small misorientation angles [7] and are difficult to be revealed by orientation sensitive etchants like nital [8]. Therefore, it is difficult to observe these lath boundaries and only the packet boundaries can be revealed clearly [9], which makes GB packets looks like grains with an almost entirely granular aspect [10]. Differently, LB forms at relatively low temperatures and consists of fine parallel laths [11]. Some of these lath boundaries are high angle grain boundaries (HAGBs) with misorientation angles higher than 15° and are prone to be revealed by etching with nital. Therefore, areas with a clear lath-like morphology correspond to LB

microstructures [9]. Despite the difference in morphology, GB is not different from LB in terms of the transformation mechanism, and both of them mainly consist of parallel laths and contain a high density of dislocations [10]. Therefore, in this research, both GB and LB are termed as bainitic ferrite (BF).

Optical micrographs of the continuously cooled microstructures with different PAGSs are shown in Figure 3. From these micrographs, we can see that the transformed microstructures with PAGSs of 22.3μm and 37.0μm are very similar and so are those with PAGSs of 52.4μm and 62.8μm. However, the transformed microstructures with PAGSs of 22.3μm and 37.0μm are quite different from those with PAGSs of 52.4μm and 62.8μm. Therefore, the PAGSs can be divided into two groups, the small PAGSs group (22.3μm and 37.0μm) and the large PAGSs group (52.4μm and 62.8μm). With the small PAGSs, the transformed microstructures are AF dominant, consisting of non-equiaxed ferrite laths with an irregular arrangement. While in the transformed microstructures with the large PAGSs, although a small fraction of AF still exists, the major transformation product is BF, organized and parallel laths nucleated on austenite grain boundaries and extended into austenite grain interior. It should be mentioned that there may be PF/QF grains in these microstructures, however, it is extremely difficult to identify them through optical microscopy or even SEM and an EBSD-based phase quantification method could be resorted to [37].
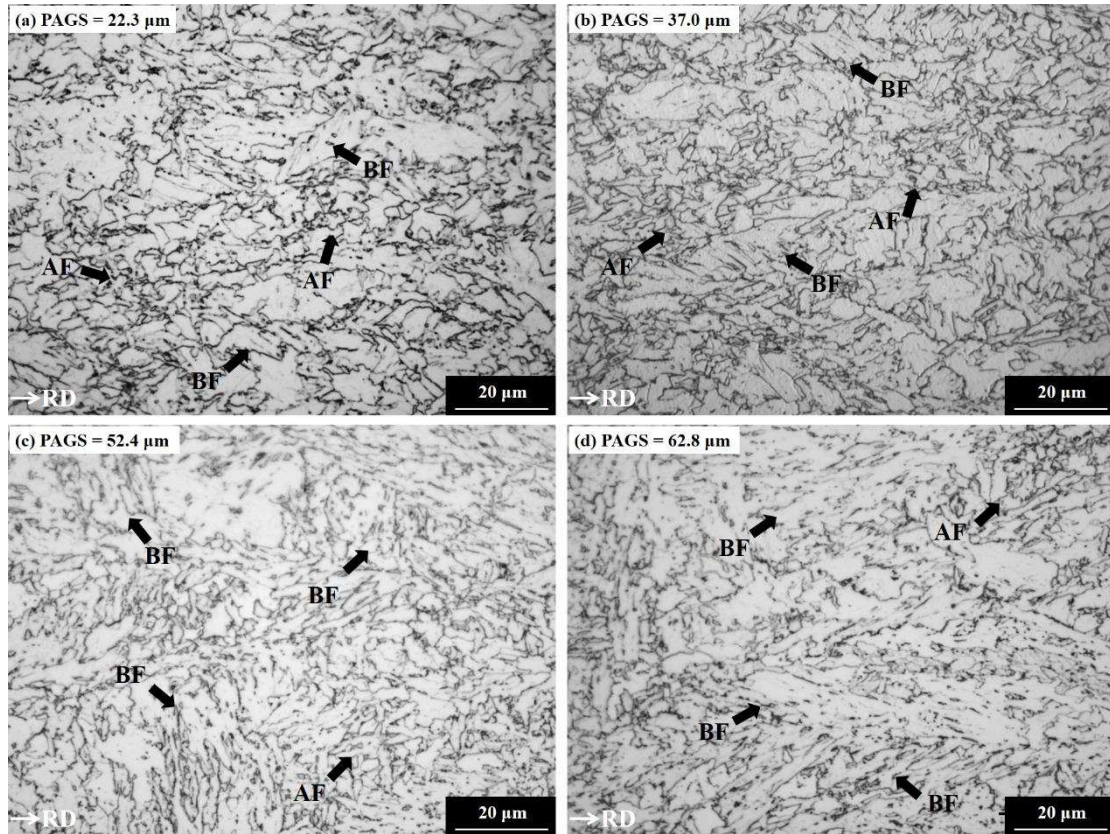
Figure 3 Optical micrographs depicting transformed microstructures with different

PAGSs: (a) 22.3μm, (b) 37.0μm, (c) 52.4μm and (d) 62.8μm.

To observe the microstructures in greater detail, SEM secondary electron micrographs of the continuously cooled microstructures with different PAGSs are shown in Figure 4. Similar results to those observed from optical micrographs can be obtained that with the small PAGSs, the transformed microstructures are AF dominant while for the large PAGSs, parallel BF laths are the main phase component. Therefore, there is a distinct effect of the PAGS before austenite deformation on the microstructure evolution under the present test condition.
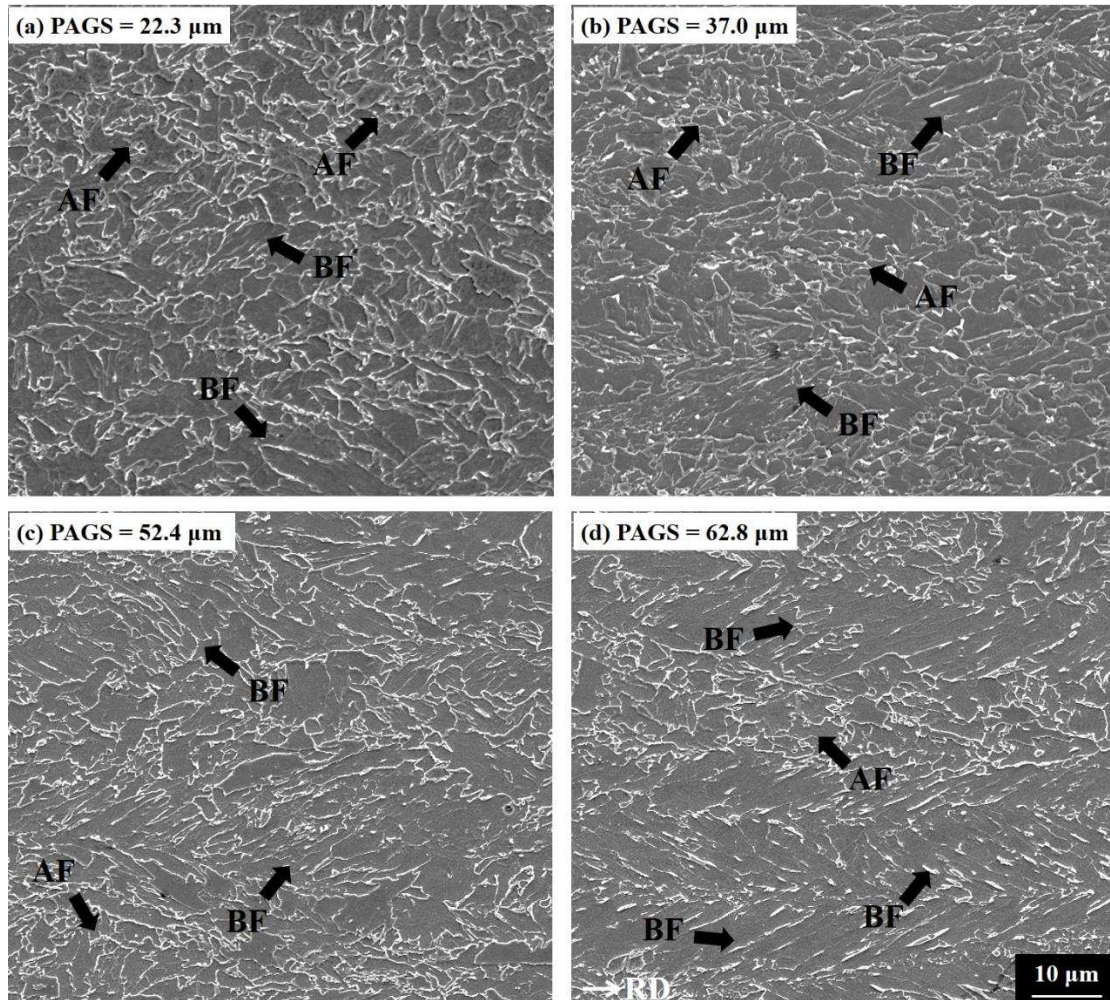
Figure 4 SEM secondary electron micrographs showing transformed microstructures with different PAGSs: (a) 22.3μm, (b) 37.0μm, (c) 52.4μm and (d) 62.8μm.

3.3 EBSD mapping

Following the noise reduction, a small area of each EBSD data set was used to plot an inverse pole figure (IPF) coloured orientation map and a boundary map. For a statistical analysis of the boundary interception length, grain size distribution and phase constitution, each whole data set was used.

The selected area IPF coloured orientation maps and corresponding boundary maps of the continuously cooled microstructures with different PAGSs are shown in Figure 5. From these maps, we can see that the transformation microstructures with the small

PAGSs (22.3μm and 37.0μm) are finer and both the densities and fractions of HAGBs are higher than those with the large PAGSs (52.4μm and 62.8μm). In the boundary maps (Figure 5e~h), the distribution of HAGBs is inhomogeneous and the whole map can be divided into two parts, regions bounded by HAGBs with a high density of LAGBs but no HAGBs inside and regions consisting of fine grains with a high density of HAGBs. One of the main differences between AF and BF is that there are a high density of HAGBs in AF [37, 38]. Although it is possible to form a high density of HAGBs in BF at low transformation temperatures [39], these HAGBs are largely generated between parallel BF laths so that they are well aligned. After a careful examination of Figure 5e~h, limited parallel HAGBs were identified, suggesting that most of the HAGBs are generated from AF transformation and the two kinds of regions can be roughly regarded as BF regions and AF regions, respectively. As shown in Figure 5e~h, fractions of BF regions are considerably higher in microstructures with the large PAGSs (Figure 5g~h), indicating that a transition from AF to BF occurs with the increase of PAGS.
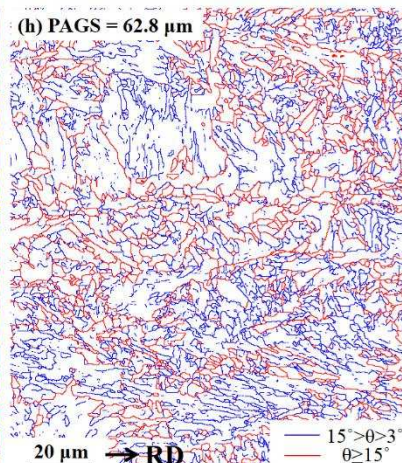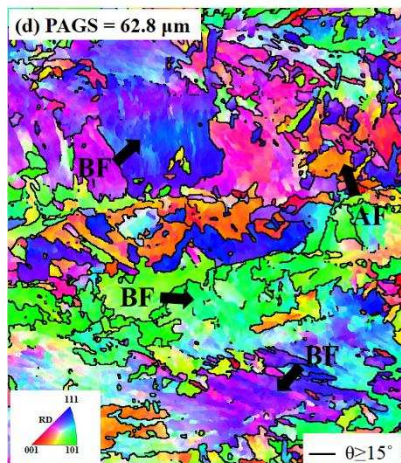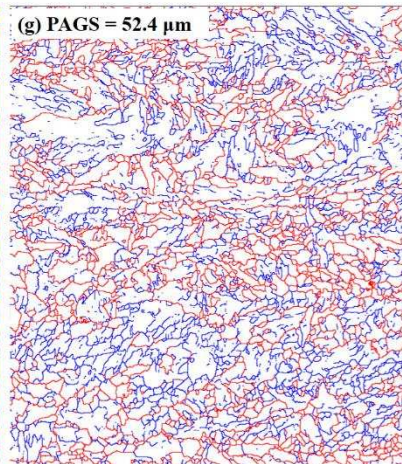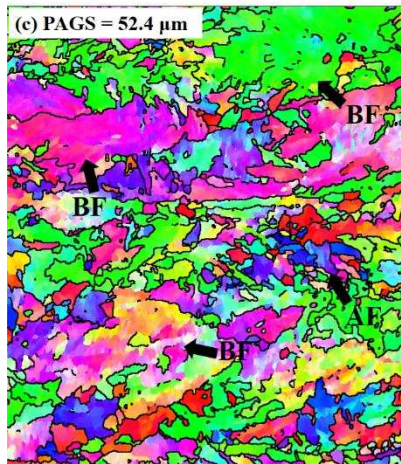
(a) PAGS = 22.3 μm
(b) PAGS = 37.0 μm
(c) PAGS = 52.4 μm
(d) PAGS = 62.8 μm
(e) PAGS = 22.3 μm
(f) PAGS = 37.0 μm
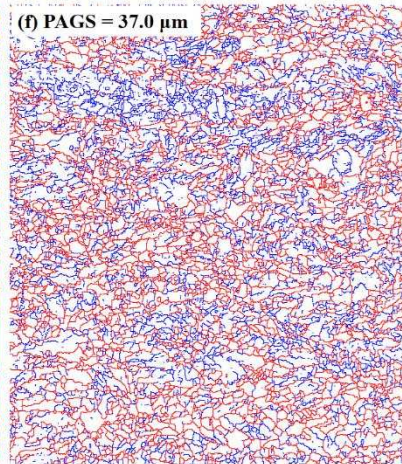(g) PAGS = 52.4 μm
(h) PAGS = 62.8 μm
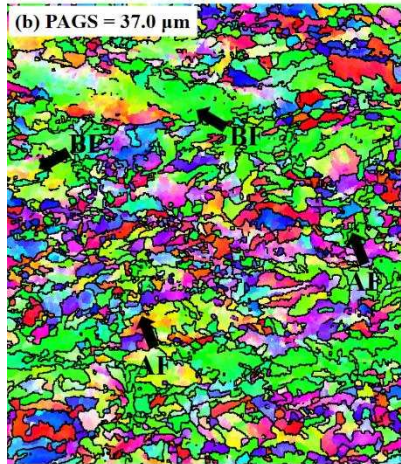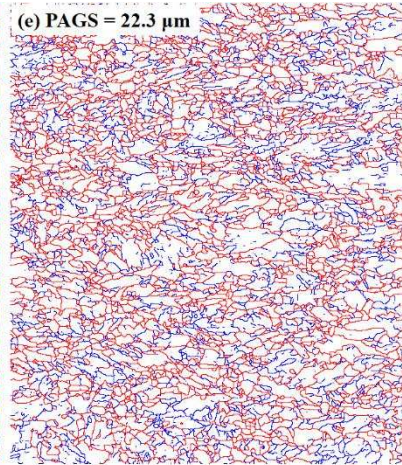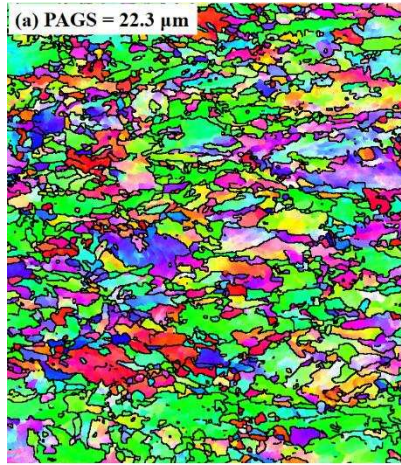
θ≥15°

20 μm → RD

15°>θ>3°
θ≥15°

Figure 5 EBSD maps of the transformed microstructures with different PAGSs: (a)~(d) inverse pole figure coloured orientation maps corresponding to microstructures with PAGS of 22.3μm, 37.0μm, 52.4μm and 62.8μm, respectively, where black lines represent high angle boundaries with misorientation greater than 15°; (e)~(h) boundary maps corresponding to the same area in (a)~(d) respectively, where blue lines represent low angle boundaries with misorientation between 3°and 15° whilst red lines represent high angle boundaries with misorientation greater than 15°.

These microstructure changes can be evaluated through a phase quantification method based on EBSD data proposed by the present authors [37]. In HSLA steels, PF/QF grains usually have equiaxed shapes, low defect densities and high fractions of HAGBs, while AF grains have small grain sizes, high defect densities and relatively high fractions of HAGBs. Based on the criteria established on grain averaged misorientation angles (defect densities), aspect ratios (grain shapes), HAGB fractions and grain sizes, fractions of PF/QF and AF grains can be quantified from the orientation maps of the transformed microstructures and the fraction of BF grains could be obtained by difference [37]. Adopting this method, fractions of PF/QF, AF and BF were quantified and the results are shown in Table 3. It is clear that with PAGS increasing from 37.0~62.8μm, the fraction of BF rises at the expense of AF and PF/QF, and a transition from AF to BF occurs. While with PAGS of 22.3μm, a relatively lower AF fraction (52.0%) can be found and possible reasons are discussed in Section 4.2.

Table 3 Fractions of different phases obtained by an EBSD based method.

PAGS(μm)	22.3	37.0	52.4	62.8
PF/QF (%)	11.6	15.1	8.3	5.4
AF (%)	52.0	57.6	34.2	31.1
BF (%)	36.4	27.3	57.5	63.5

To quantify the microstructure refinement, misorientation angle threshold values should be selected. Misorientation angles of 4° and 15° are typical threshold values to define the microstructural unit sizes responsible for strengthening and toughening, respectively [40, 41]. Grain sizes defined by different misorientation threshold values, 4° and 15°, were measured by a linear intercept method in the Channel 5 software, respectively. The geometric means of the linear intercept lengths in both horizontal and vertical directions were calculated as in reference [35] and are shown in Figure 6. It can be seen in Figure 6 that the mean linear intercept lengths following both misorientation angle threshold values firstly decrease with the reduction of PAGS from 62.8μm to 37.0μm and then level off when PAGS is further reduced to 22.3μm. Furthermore, changes of the mean intercept lengths both between the transformed microstructures with PAGSs of 52.4μm and 62.8μm and between the transformed microstructures with PAGSs of 22.3μm and 37.0μm are not statistically significant as there are very large overlaps of the error bars. But the difference of the mean intercept length is quite evident between the transformed microstructures with the small and the large PAGSs.
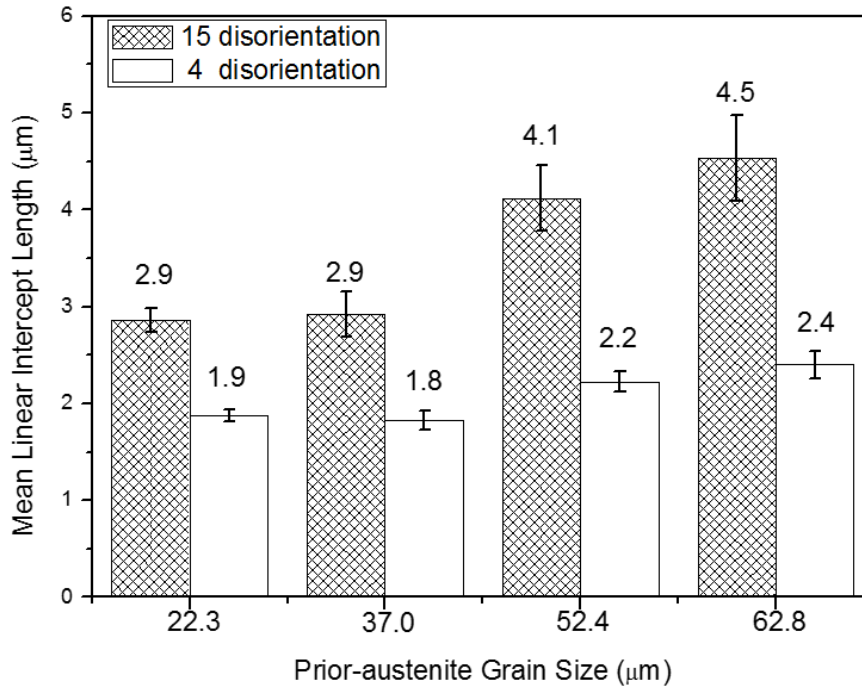
Figure 6 Microstructure size parameters measured against two misorientation criteria, 4° and 15°, as the geometric means of the linear interception lengths in horizontal and vertical directions from the EBSD maps of the transformed microstructures with different PAGSs. Error bars represent 95% confidence levels of the measurement.

By altering the PAGS before austenite deformation, not only the grain refinement but also the microstructure homogeneity are influenced as shown in Figure 5. In order to quantify the microstructure homogeneity, the distributions of grain sizes defined by the diameter of the equivalent circle against the misorientation angle criteria of 15° for the transformed microstructures with different PAGSs are shown in Figure 7. With the small PAGSs (22.3μm and 37.0μm), the AF dominant microstructures possess homogeneous grain size distributions and the difference between them is very small. As PAGS is increased from 37.0μm to 62.8μm, an increase in the microstructure

heterogeneity is observed and with the largest PAGS (62.8μm) the grain size distribution is the wildest. Therefore, it is straightforward to say that reducing PAGS before austenite deformation can significantly homogenise the transformed microstructure.
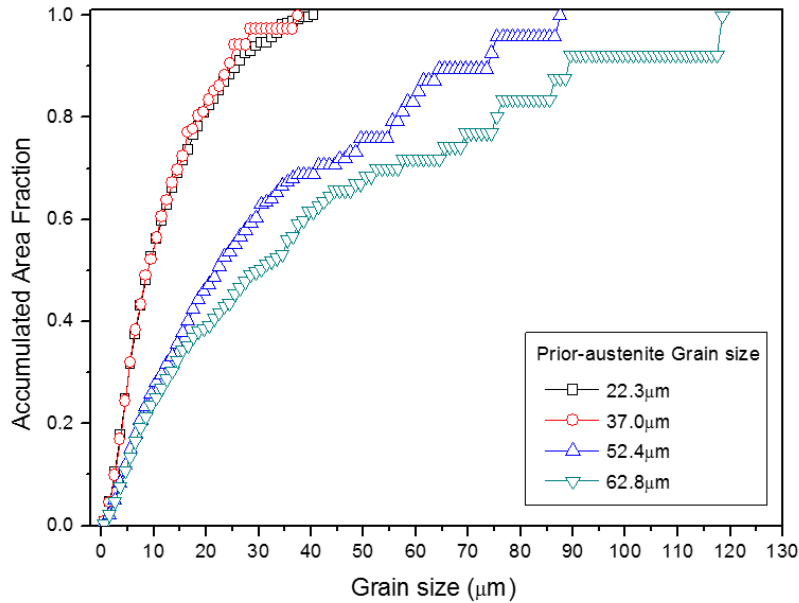
Figure 7 Grain size distributions of the transformed microstructures with different PAGSs against the misorientation angle criteria of 15° plotted in terms of accumulated area fraction.

4. Discussion

4.1 Effect of PAGS on AF transformation

Since AF in HSLA steels is widely considered as an intragranularly nucleated transformation product, according to the results of research [29, 30] that by increasing PAGS, the dominant transformation product changes from boundary nucleated phases, e.g. BF, to intragranular nucleated phases, the volume fraction of AF in HSLA steels

should be raised with the increase of PAGS. However, as shown in Table 3 that the volume fraction of AF actually is reduced with the increase of PAGS from 37.0μm to 62.8μm. The discrepancy between the experimental results in this research and those in reference [29, 30] can be attributed to the difference in intragranular nucleation sites between AF in steel welds and AF in HSLA steels.

It is universally acknowledged that AF in steel welds nucleates on the non-metallic inclusions introduced during welding, and after welding, the density of the non-metallic inclusions and thus the possible nucleation sites of AF is fixed. With regard to BF, prior-austenite grain boundaries are its nucleation sites and for recrystallised austenite grains, the total area of austenite grain boundaries per unit volume, S_v, was proposed as:

$$S_v = \frac{2}{D} \tag{1}$$

where D is the austenite grain size measured by the mean linear intercept length [42]. Therefore, the nucleation site density of BF increases reciprocally with the reduction of PAGS while that of AF in steel welds remains fixed, leading to the promotion of the boundary nucleated phase (BF) and thus the reduction of the intragranularly nucleated phase (AF) in steel welds as shown in research [29, 30].

In contrast, the reduction of AF fraction with the increase of PAGS found in this research can be explained by considering the change of nucleation site densities of AF and BF with the rise of PAGS. As proposed by the present authors [31], the introduction of intragranular nucleation sites and the halting of BF laths nucleated on austenite grain boundaries are the two conditions should be fulfilled for the occurrence of acicular ferrite transformation in HSLA steels. Austenite deformation is critical to meet these

two conditions as it introduces a high density of dislocations that act as intragranular nucleation sites for AF and these deformation substructures also suppress the lengthening of BF laths through the mechanism of mechanical stabilisation of austenite [43-45]. Therefore, the density of deformation induced dislocations can be approximately regarded as the nucleation site density of AF. The density of deformation induced dislocation, ρ, was presented as:

$$\rho = \frac{C\varepsilon}{bl} \tag{2}$$

where C is a constant, ε the strain, b the magnitude of the Burgers vector and l the average slip length [46]. The average slip length must decrease as the plastic strain increases and was proposed as:

$$l = \frac{\delta D}{(\delta + D\varepsilon)} \tag{3}$$

where D is the austenite grain size before deformation, ε the strain and δ a coefficient equal to ~1μm [47]. Combining Equation (2) and (3), the dislocation density can be expressed as:

$$\rho = \frac{C\varepsilon}{bD} + \frac{C\varepsilon^2}{b\delta} \tag{4}$$

It is apparent that the dislocation density increases reciprocally with the reduction of PAGS before deformation. This is also in accordance with the result indicated by the Hall-Petch relationship [48] and the relationship between the stress and the dislocation density proposed as:

$$\sigma = \alpha Gb\rho^{1/2} \tag{5}$$

where α is a numerical constant of order unity and G the shear modulus [49].

With regard to BF, prior-austenite grain boundaries can be treated as its nucleation sites and the total area of deformed austenite grain boundary per unit volume, S_v(GB), was presented as:

$$S_v(\text{GB}) = [1.67(R - 0.1) + 1](\frac{2}{D}) \qquad (6)$$

where R is the reduction ratio [50]. From Equation (6) we could see that under the same reduction ratio, namely the same strain2, the total area of deformed austenite grain boundaries per unit volume also has a reciprocal relationship with the change of PAGSs.

Based on Equation (4) and (6), it is clear that unlike AF in steel welds, although the nucleation site density of BF increases reciprocally with the reduction of PAGS, the nucleation site density of AF in HSLA steels also rises with a reciprocal relationship with the decrease of PAGS. More importantly, compared with AF, BF laths are more likely to be suppressed by austenite deformation substructures and austenite grain boundaries. For BF microstructures with the large PAGSs and thus the low dislocation densities, BF laths nucleate on austenite grain boundaries and extend into the austenite grain interior. The lengthening of BF laths is more likely to be halted by the opposite austenite grain boundaries or by the BF laths nucleated on the opposite austenite grain boundaries. Therefore, long BF laths and large BF packets were developed as shown in Figure 5c~d. With the reduction of PAGS, the areas in austenite grains become smaller and narrower after deformation. This restricts BF laths and packets to smaller sizes because displacive transformation interfaces cannot move through the austenite grain boundaries [11]. Moreover, due to the higher dislocation densities in deformed small-grained austenite, BF laths are more likely to be suppressed by deformation

substructures through the mechanism of mechanical stabilization of austenite [43-45]. Both of these two factors lead to dramatically decreased BF lath lengths and packet sizes as shown in Figure 5a~b. On the other hand, for AF microstructures, it is the impingement between adjacently nucleated AF laths instead of austenite deformation substructures and austenite grain boundaries that suppresses the lengthening of AF laths, so that AF grains in all transformed microstructures have small grain sizes (Figure 5a~d). Therefore, compared with AF laths, BF laths are more susceptible to the mechanical stabilisation effect of austenite deformation substructures and the restricting effect of austenite grain boundaries.

It should be noted as well that decreasing PAGS before austenite deformation also compromises the hardenability of HSLAs steels, which can be manifested by the increased PF/QF fractions shown in Table 3, with PAGS decreasing from 52.4μm to 37.0μm. The formation of PF/QF grains occupies the austenite grain boundaries which could be the nucleation site of BF. Furthermore, the enrichment of carbon or carbon and substitutional solid solution elements in the surrounding austenite stabilises the austenite and postpones the BF nucleation on α/γ interfaces [29, 30]. In contrast, this enrichment has a less severe impact on AF transformation due to its intragranular nucleation.

In summary, although both the nucleation site densities of BF and AF increase reciprocally with the reduction of PAGS, Equation (4) and (6), BF laths are subjected to increasingly severe mechanical stabilisation effect of austenite deformation substructures and restricting effect of austenite grain boundaries, which significantly

suppresses the lengthening of BF laths. The increased fraction of PF/QF grains also take up the austenite grain boundaries and postpone the BF nucleation on α/γ interfaces. All of these factors lead to the decreased BF fractions and increased AF fractions with the reduction of PAGS from 62.8μm to 37.0μm. The increased fraction of AF and the reduction of BF packet sizes with the decreased PAGS both improves the microstructure refinement and homogeneity as shown in Figure 6 and Figure 7.

Based on the illustrations above, the relatively smaller influence of reducing PAGS from 62.5μm to 52.4μm than decreasing PAGS from 52.4μm to 37.0μm on the microstructure evolution (Table 3) and grain refinement (Figure 6) can also be explained by the reciprocal relationship between the deformed austenite dislocation density and the change of PAGSs as schematically illustrated in Figure 8.
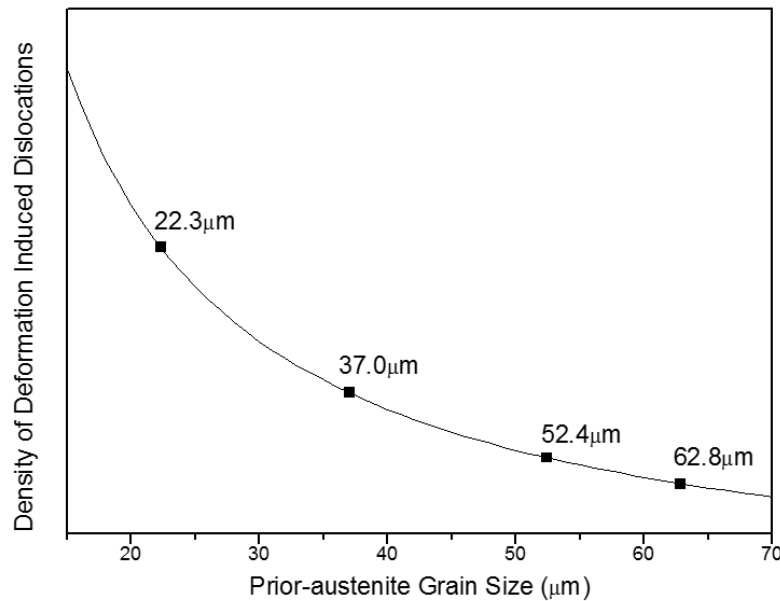

Figure 8 Schematical illustration of the reciprocal relationship between the density of deformation induced dislocations and the PAGS before deformation.

Although some researchers still claimed that AF in HSLA steels nucleates on non-metallic inclusions [51], the results in this research that the fraction of AF is increased with the reduction of PAGS, add an indirect evidence that the intragranular nucleation sites of AF in HSLA steels are deformation substructures instead of non-metallic inclusions. Furthermore, the advances in steel making technology have significantly improved the cleanness of modern high strength low alloy (HSLA) steels and a high purity is also a prerequisite for modern HSLA steels. Clean steels are characterized by very small amounts of oxides and sulfides [52] and it is difficult to find high enough quantity of non-metallic inclusions in high grades HSLA steels, especially pipeline steels, to support AF transformation as in steel weld.

4.2 Cease of grain refinement with PAGS of 22.3μm

Although as PAGS is decreased from 62.8μm to 37.0μm the fraction of AF is increased (Table 3) and the transformed microstructure is refined (Figure 6), reducing PAGS further to 22.3μm, the fraction of AF is not increased and the transformed microstructure is not refined as shown in Table 3 and Figure 6, respectively. Since the fraction of AF and microstructure refinement both are closely related to the density of deformation induced dislocations, it is reasonable to argue that as PAGS is reduced from 37.0μm to 22.3μm, the trend that deformation induced dislocations increase as schematically illustrated in Figure 8 is weakened or prohibited due to the operation of certain mechanisms.

It is well known that under the same deformation conditions, decreasing the starting austenite grain size, the critical strain for the onset of dynamic recrystallization

(DRX) is reduced [53] and once DRX is triggered during the deformation, not necessary to a large extent, static recrystallization (SRX) and meta-dynamic recrystallization (MDRX) can proceed during the following continuous cooling and result in an evident restoration as shown in research [54]. Therefore, it is reasonable to conceive that with PAGS of 22.3μm, DRX was triggered during the austenite deformation and resulted in a decrease of the dislocation density. However, after strain2 of 0.5, the austenite grains remain unrecrystallised as shown in Figure 2e which means that DRX is not triggered during the austenite deformation with PAGS of 22.3μm.

SRX could still happen during the subsequent continuous cooling. Under the cooling conditions used in this research, displacive transformations (AF and BF) dominate. The continuously cooled specimen with PAGS of 22.3μm was etched with a saturated aqueous picric acid solution to reveal the PAGBs. The optical micrograph depicting the PAGBs before phase transformation is shown in Figure 9. As can be seen from this figure, the shape of the prior-austenite grains cannot be observed clearly. Therefore, it is difficult to determine whether SRX happens during the continuous cooling directly from the optical micrograph of the PAGBs.
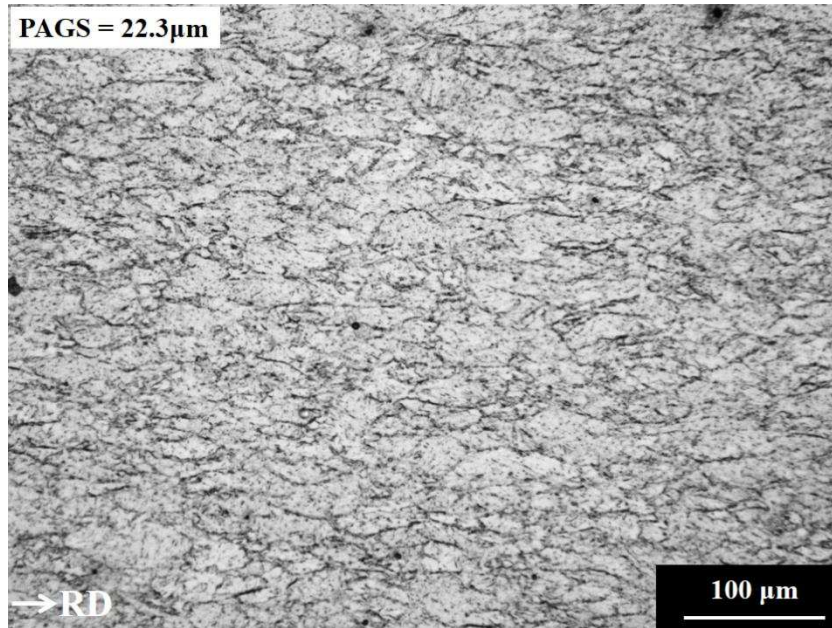
Figure 9 Optical micrograph depicting prior-austenite grain boundaries of the

continuously cooled specimen with PAGS of 22.3μm.

Alternatively, the texture information of the transformed microstructure can be used as an indicator to see whether SRX occurs during the continuous cooling. The principal texture component presented in the recrystallised austenite is the cube ({001}<010>) texture component and after displacive transformations, its products are the Goss ({110} <001>), the rotated Goss ({110} <110>) and the rotated cube ({001}<110>) texture components [55]. The presence of the Goss and the rotated Goss texture components is a sign that austenite is recrystallised or partially recrystallised before transformation and the presence of the rotated cube texture component alone does not necessarily indicate the occurrence of austenite recrystallization because the rotated cube texture component can also be transformed from the Brass ({110} <112>) texture component [55]. The texture of the transformation product with PAGS of

22.3μm is represented by the $\varphi_2=45°$ section of ODF (Figure 10a), and positions of the relevant texture components in the $\varphi_2=45°$ section are shown in Figure 10b. From Figure 10 we can see that although the rotated cube texture component exists in the texture of the transformed microstructure, the absence of the Goss and the rotated Goss texture components suggests that austenite was unrecrystallised before transformation even with PAGS as small as 22.3μm. Therefore, both DRX and SRX did not happen in the present research and thus are not responsible for the cease of microstructure refinement when PAGS is reduced from 37.0μm to 22.3μm.
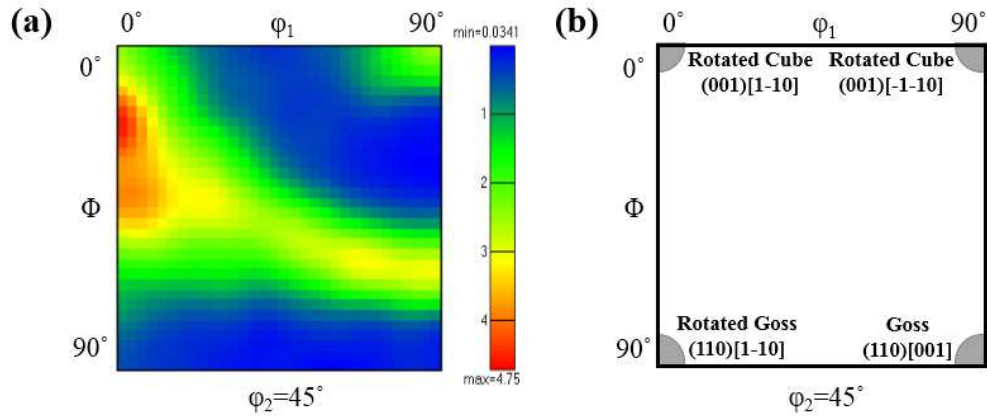
Figure 10 (a) $\varphi_2=45°$ section of the ODF measured by EBSD technique for the transformed microstructure with PAGS of 22.5μm, (b) positions of the relevant texture components in the $\varphi_2=45°$ section.

The experimental results in research [56, 57] may provide an explanation for the cease of microstructure refinement when PAGS is reduced from 37.0μm to 22.3μm. In research [56] after AISI 304 stainless steel specimens with PAGSs of 40μm and 15μm were deformed with a strain of 1.0 at 900°C and a strain rate of 0.5s^{-1}, uniformly distributed substructures can be found in the unrecrystallised coarse-grained austenite,

while in the fine-grained austenite, relatively dense substructures exist only near the austenite grain boundaries, leaving the interior lack of sub-grain boundaries. Similarly, in research [57], after AISI 304 stainless steel specimens with PAGSs of 35μm and 8μm were deformed at 900°C with a strain of 1.0 and a strain rate of $0.01s^{-1}$, it was found that in the coarse-grained austenite two types of deformation substructures exist, dense cell structures and elongated dislocation boundaries with large distances between them, but in fine-grained austenite the major part of substructures are the elongated dislocation boundaries and the density of substructures is significantly less than that in the coarse-grained austenite. As for the reason of these differences, it was proposed that during the deformation of the fine-grained austenite, grain boundary shearing and/or sliding take place at austenite grain boundaries which leads to the development of inhomogeneous deformation substructures near the grain boundaries and in the fine-grained austenite, dynamic recovery is promoted due to the acceleration of dislocations spreading into austenite grain boundaries [56, 57].

Based on the results of these investigations [56, 57], it is clear that the type, distribution, and density of the deformation substructures are different as PAGS reduces from 40μm to 15μm or from 35 μm to 8 μm. Therefore, a similar change in the deformation substructures could be expected in the present research with the reduction of PAGS from 37.0μm to 22.3μm and it could be these changes that are responsible for the cease of microstructure refinement. However, further investigations on the austenite deformation substructure with small PAGSs in model alloys possessing similar stacking fault energy to HSLA steels are required.

4.3 Effective grain sizes

The grain size measured against the high misorientation angle (15˚), $d_{15˚}$, is usually called the effective grain size. Effective grain size is a very important microstructural parameter because it is an indicator of the density of high angle grain boundaries ($\theta \geq 15˚$) which provide effective barriers to cleavage fracture by arresting cracks or deviating their propagation directions [58, 59]. Therefore it is imperative to establish a relationship between processing parameters and effective grain sizes.

The parameter S_v was originally proposed to quantify the total effective nucleation sites area per unit volume for ferrite transformation [60] and a reciprocal relationship between ferrite grain sizes and S_v values in both recrystallised and deformed austenite were found in research [60]. Therefore, increasing S_v is the primary method to refine ferrite microstructures. Accordingly, the parameter, S_v, is used here to reveal the relationship between effective grain sizes and S_v values. For recrystallised austenite, S_v was calculated by Equation (1), while for deformed austenite, S_v was proposed as:

$$S_v = S_v(GB) + S_v(DB)$$
$$= [1.67(R - 0.1) + 1](\frac{2}{D}) + 0.63(R - 0.3) \tag{7}$$

where S_v(GB) stands for the total area of deformed austenite grain boundary per unit volume, S_v(DB) the total area of intragranular planar defects per unit volume, D the austenite grain size and R the reduction ratio [50]. Based on the effective grain sizes of specimens with different PAGSs and different strain2 but undergone the same accelerated cooling process (10˚C/s), the relationship between effective grain sizes and S_v values of the tested steel in this research is shown in Figure 11. Like the results in

research [60] for ferrite grain sizes, effective grain sizes of the transformed microstructures have a reciprocal relationship with S_v values. Although S_v was originally proposed to quantify the total effective nucleation site area of ferrite per unit volume [60] and the nucleation site density of AF cannot be accurately quantified by the S_v value, the factors affecting the nucleation site density of AF, including PAGSs and austenite strain volumes, are also included in the expressions of S_v for deformed austenite, Equation(7).
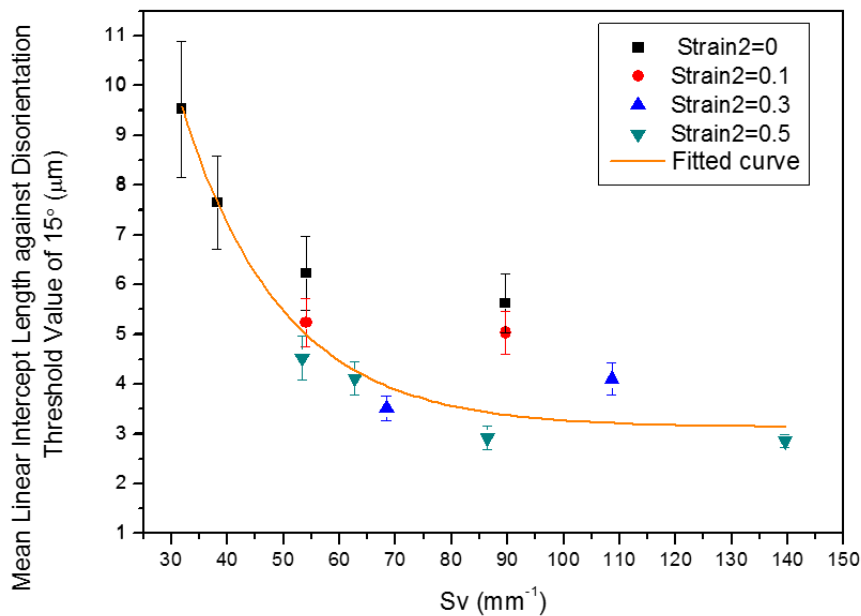
Figure 11 Relationship between the effective grain size of transformed microstructure after an accelerated cooling (10˚C/s) and the S_v value.

Some discrepancies can also be identified in Figure 11. With nearly the same S_v values (around 55mm^{-1} and 90mm^{-1}), the effective grain sizes of recrystallised (strain2 of 0), slightly deformed (strain2 of 0.1) and largely deformed austenite (strain2 of 0.5) are quite different and these differences raise with the increased S_v values. Therefore,

with the same S$_v$ value, deformation of austenite with a large austenite grain size is more effective than refining austenite grain size to a smaller value but without deformation in refining transformed microstructures and this advantage of austenite deformation is more evident at higher S$_v$ values. Therefore, a reasonable allocation of total rolling reduction to rough rolling and finish rolling is required to achieve small effective grain sizes.

Alternatively, by analysing the effective grain sizes obtained with the same steel composition (Table 1) but different processing parameters [31, 34, 37, 54], an equation relating effective grain sizes with processing parameters was proposed as:

$$d_{15°} = 3.37 \times 10^{-3}D^2 \exp(-3\varepsilon)\,\dot{T}^{-0.1} + 2.31 \tag{8}$$

where D is the austenite grain size within the range of 22.3~63.7μm, ε the austenite strain volume between 0 and 0.5 and $\dot{T}$ the cooling rate changing from 5˚C/s to 20˚C/s. The experimental effective grain sizes and the equation calculated values are shown in Figure 12 and a reasonable consistency can be found.
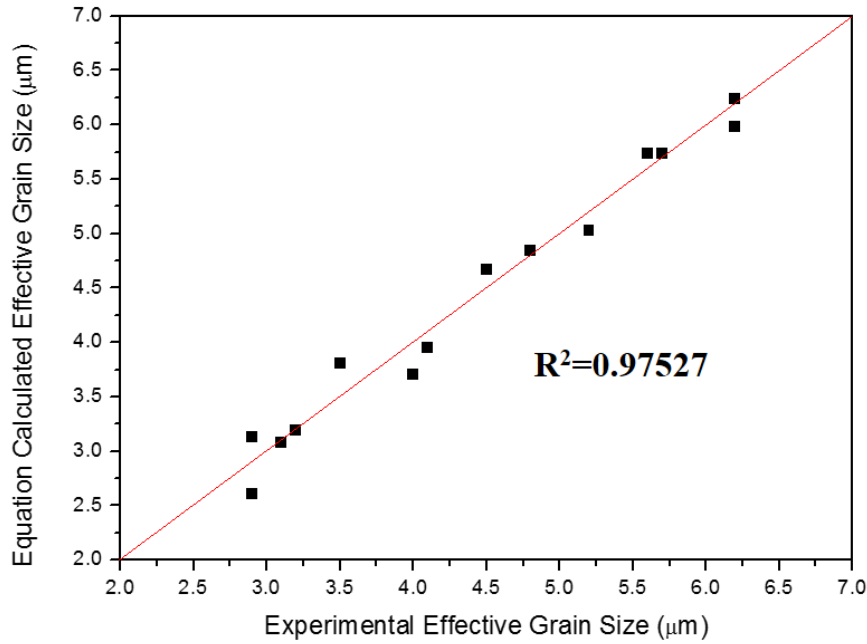
Figure 12 Experimental and Equation calculated effective grain sizes.

5. Conclusion

In this research, different parameters of solid-solution heat treatment and rough deformation were used to generate austenite with different grain sizes and the effects of austenite grain size before deformation on the acicular ferrite transformation and grain refinement were investigated. It was found that:

(1) With the small PAGSs (22.3μm and 37.0μm), the transformed microstructures are AF dominant, while with the large PAGSs (52.4μm and 62.8μm), although a small fraction of AF still exists, the major transformation product is BF. As PAGS is reduced, the transformed microstructure is refined and homogenised.

(2) Although both the nucleation site densities of BF and AF increase reciprocally with the reduction of PAGS, BF laths are subjected to increasingly severe

mechanical stabilisation effect of austenite deformation substructures and restricting effect of austenite grain boundaries, which significantly suppress the lengthening of BF laths. The increased fraction of PF/QF grains also take up the austenite grain boundaries and postpone the BF nucleation on α/γ interfaces. All of these factors lead to the decreased BF fractions and increased AF fractions with the reduction of PAGS from 62.8μm to 37.0μm.

(3) Reducing PAGS further from 37.0μm to 22.3μm, the fraction of AF is not increased and the transformed microstructure is not refined. Occurrence of restoration processes like DRX and SRX is excluded and possible differences in the type, distribution, and density of the deformation substructures between deformed austenite with PAGSs of 37.0μm and 22.3μm are proposed to be responsible for the cease of microstructure refinement.

(4) Based on the effective grain sizes obtained with the same steel composition but different processing parameters, a reciprocal relationship between effective grain sizes and S_v values were found and an equation relating effective grain sizes with processing parameters was proposed.

Acknowledgements

Data availability

The raw/processed data required to reproduce these findings cannot be shared at this time as the data also forms part of an ongoing study.

Reference

[1] M.C. Zhao, K. Yang, Y. Shan, The effects of thermo-mechanical control process on microstructures and mechanical properties of a commercial pipeline steel, Mater. Sci. Eng. A 335 (2002) 14-20.

[2] S. Shanmugam, N. Ramisetti, R. Misra, J. Hartmann, S. Jansto, Microstructure and high strength–toughness combination of a new 700MPa Nb-microalloyed pipeline steel, Mater. Sci. Eng. A 478 (2008) 26-37.

[3] Y.M. Kim, S.K. Kim, Y.J. Lim, N.J. Kim, Effect of microstructure on the yield ratio and low temperature toughness of linepipe steels, ISIJ Int. 42 (2002) 1571-1577.

[4] R. Zhang, J. Boyd, Bainite transformation in deformed austenite, Metall. Mater. Trans. A 41 (2010) 1448-1459.

[5] W. Wang, Y. Shan, K. Yang, Study of high strength pipeline steels with different microstructures, Mater. Sci. Eng. A 502 (2009) 38-44.

[6] M.C. Zhao, B. Tang, Y.Y. Shan, K. Yang, Role of microstructure on sulfide stress cracking of oil and gas pipeline steels, Metall. Mater. Trans. A 34 (2003) 1089-1096.

[7] Y. Zhong, F. Xiao, J. Zhang, Y. Shan, W. Wang, K. Yang, In situ TEM study of the effect of M/A films at grain boundaries on crack propagation in an ultra-fine acicular ferrite pipeline steel, Acta Mater. 54 (2006) 435-443.

[8] C. Chiou, J. Yang, C. Huang, The effect of prior compressive deformation of austenite on toughness property in an ultra-low carbon bainitic steel, Mater. Chem. Phys. 69 (2001) 113-124.

[9] S. Babu, H. Bhadeshia, Transition from bainite to acicular ferrite in reheated Fe–Cr–C weld deposits, Mater. Sci. Tech. 6 (1990) 1005-1020.

[10] L. Cheng, K.M. Wu, New insights into intragranular ferrite in a low-carbon low-alloy steel, Acta Mater. 57 (2009) 3754-3762.

[11] H.K.D.H. Bhadeshia, Bainite in steels, Inst. of Metals1992.

[12] Y. Smith, A. Coldren, R. Cryderman, Manganese-Molybdenum-Niobium Acicular Ferrite Steels with High Strength and Toughness, Toward improved ductility and toughness, Climax Molybdenum Company (Japan) Ltd, Kyoto, 1972, pp. 119-142.

[13] Y.M. Kim, H. Lee, N.J. Kim, Transformation behavior and microstructural characteristics of acicular ferrite in linepipe steels, Mater. Sci. Eng. A 478 (2008) 361-370.

[14] J. Yang, H. Bhadeshia, Orientation relationships between adjacent plates of acicular ferrite in steel weld deposits, Mater. Sci. Tech. 5 (1989) 93-97.

[15] S. Babu, H. Bhadeshia, Stress and the acicular ferrite transformation, Mater. Sci. Eng. A 156 (1992) 1-9.

[16] Z. Tang, W. Stumpf, The role of molybdenum additions and prior deformation on acicular ferrite formation in microalloyed Nb–Ti low-carbon line-pipe steels, Mater. Charact. 59 (2008) 717-728.

[17] Y.M. Kim, S.Y. Shin, H. Lee, B. Hwang, S. Lee, N.J. Kim, Effects of molybdenum and vanadium addition on tensile and charpy impact properties of API X70 linepipe steels, Metall. Mater. Trans. A38 (2007) 1731-1742.

[18] S. Lee, D. Kwon, Y.K. Lee, O. Kwon, Transformation strengthening by thermomechanical treatments in C-Mn-Ni-Nb steels, Metall Mater Trans A 26 (1995) 1093-1100.

[19] S. Yamamoto, H. Yokoyama, K. Yamada, M. Niikura, Effects of the austenite grain size and deformation in the unrecrystallized austenite region on bainite transformation behavior and

microstructure, ISIJ Int. 35 (1995) 1020-1026.

[20] J. Yang, C. Huang, C. Chiou, The influence of plastic deformation and cooling rates on the microstructural constituents of an ultra-low carbon bainitic steel, ISIJ Int. 35 (1995) 1013-1019.

[21] D. Bai, S. Yue, T. Maccagno, J. Jonas, Effect of deformation and cooling rate on the microstructures of low carbon Nb-B steels, ISIJ Int. 38 (1998) 371-379.

[22] F.R. Xiao, B. Liao, Y.Y. Shan, G.Y. Qiao, Y. Zhong, C. Zhang, K. Yang, Challenge of mechanical properties of an acicular ferrite pipeline steel, Mater. Sci. Eng. A 431 (2006) 41-52.

[23] S.-b. Yin, X.-j. Sun, Q.-y. Liu, Z.-b. Zhang, Influence of Deformation on Transformation of Low-Carbon and High Nb-Containing Steel During Continuous Cooling, J. Iron Steel Res. Int. 17 (2010) 43-47.

[24] P. Cizek, B.P. Wynne, C.H.J. Davies, P.D. Hodgson, The Effect of Simulated Thermomechanical Processing on the Transformation Behavior and Microstructure of a Low-Carbon Mo-Nb Linepipe Steel, Metall. Mater. Trans. A 46 (2014) 407-425.

[25] P. Cizek, B. Wynne, C.H.J. Davies, B. Muddle, P. Hodgson, Effect of composition and austenite deformation on the transformation characteristics of low-carbon and ultralow-carbon microalloyed steels, Metall. Mater. Trans. A 33 (2002) 1331-1349.

[26] A. Garcia-Junceda, C. Capdevila, F. Caballero, C.G. de Andrés, Dependence of martensite start temperature on fine austenite grain size, Scripta Mater. 58 (2008) 134-137.

[27] M. Umemoto, N. Komatsubara, I. Tamura, Prediction of hardenability effects from isothermal transformation kinetics, Journal of Heat Treating 1 (1980) 57-64.

[28] A. Matsuzaki, H. Bhadeshia, Effect of austenite grain size and bainite morphology on overall kinetics of bainite transformation in steels, Mater. Sci. Tech. 15 (1999) 518-522.

[29] R. Farrar, Z. Zhang, S. Bannister, G. Barritte, The effect of prior austenite grain size on the transformation behaviour of C-Mn-Ni weld metal, J. Mater. Sci. 28 (1993) 1385-1390.

[30] S. Babu, H. Bhadeshia, Mechanism of the transition from bainite to acicular ferrite, Materials Transactions, JIM(Japan) 32 (1991) 679-688.

[31] H. Zhao, B.P. Wynne, E.J. Palmiere, Conditions for the occurrence of acicular ferrite transformation in HSLA steels, J. Mater. Sci. 53 (2018) 3785–3804.

[32] H. Zhao, Effect of Austenite Deformation and Continuous Cooling on the Microstructural Evolution in a Microalloyed Steel, Ph.D Thesis, University of Sheffield, 2016.

[33] C. Heckmann, D. Ormston, F. Grimpe, H.G. Hillenbrand, J.P. Jansen, Development of low carbon Nb–Ti–B microalloyed steels for high strength large diameter linepipe, Ironmak. Steelmak. 32 (2005) 337-341.

[34] H. Zhao, B.P. Wynne, E.J. Palmiere, Effect of austenite grain size on the bainitic ferrite morphology and grain refinement of a pipeline steel after continuous cooling, Mater. Charact. 123 (2017) 128-136.

[35] L. Sun, M. Thomas, B.P. Wynne, E.J. Palmiere, K. Mingard, B. Roebuck, Mapping microstructure inhomogeneity using electron backscatter diffraction in 316L stainless steel subjected to hot plane strain compression tests, Mater. Sci. Technol. 26 (2010) 1477-1486.

[36] K. Hulka, J. Gray, High Temperature Processing of Line Pipe Steels, Proceedings of the International Symposium Niobium, 2001, pp. 587-612.

[37] H. Zhao, B.P. Wynne, E.J. Palmiere, A phase quantification method based on EBSD data for a continuously cooled microalloyed steel, Mater. Charact. 123 (2017) 339-348.

[38] S.L. Shrestha, A.J. Breen, P. Trimby, G. Proust, S.P. Ringer, J.M. Cairney, An automated method of

quantifying ferrite microstructures using electron backscatter diffraction (EBSD) data, Ultramicroscopy 137 (2014) 40-7.

[39] N. Takayama, G. Miyamoto, T. Furuhara, Effects of transformation temperature on variant pairing of bainitic ferrite in low carbon steel, Acta Mater. 60 (2012) 2387-2396.

[40] L. Fan, D. Zhou, T. Wang, S. Li, Q. Wang, Tensile properties of an acicular ferrite and martensite/austenite constituent steel with varying cooling rates, Mater. Sci. Eng. A 590 (2014) 224-231.

[41] N. Isasti, D. Jorge-Badiola, M.L. Taheri, P. Uranga, Phase transformation study in Nb-Mo microalloyed steels using dilatometry and EBSD quantification, Metall. Mater. Trans. A 44 (2013) 3552-3563.

[42] A. Thorvaldsen, The intercept method—2. Determination of spatial grain size, Acta Mater. 45 (1997) 595-600.

[43] P. Shipway, H. Bhadeshia, Mechanical stabilisation of bainite, Mater. Sci. Tech. 11 (1995) 1116-1128.

[44] S. Singh, H. Bhadeshia, Quantitative evidence for mechanical stabilization of bainite, Mater. Sci. Tech. 12 (1996) 610-612.

[45] S. Chatterjee, H.-S. Wang, J. Yang, H. Bhadeshia, Mechanical stabilisation of austenite, Mater. Sci. Tech. 22 (2006) 641-644.

[46] M. Ashby, The deformation of plastically non-homogeneous materials, Philos. Mag. 21 (1970) 399-424.

[47] F. Barlat, M. Glazov, J. Brem, D. Lege, A simple model for dislocation behavior, strain and strain rate hardening evolution in deforming aluminum alloys, Int. J. Plasticity. 18 (2002) 919-939.

[48] M.F. Ashby, The deformation of plastically non-homogeneous materials, Philos. Mag. 21 (1970) 399-424.

[49] H. Mecking, U. Kocks, Kinetics of flow and strain-hardening, Acta Metall. 29 (1981) 1865-1875.

[50] C. OUCHI, T. SAMPEI, I. KOZASU, The Effect of Hot Rolling Condition and Chemical Composition on the Onset Temperature of γ-α Transformation after Hot Rolling, Transactions of the Iron and Steel Institute of Japan 22 (1982) 214-222.

[51] C. Liu, L. Shi, Y. Liu, C. Li, H. Li, Q. Guo, Acicular ferrite formation during isothermal holding in HSLA steel, J. Mater. Sci. 51 (2016) 3555-3563.

[52] R. Cochrane, The effect of second-phase particles on the mechanical properties of steel, The Iron and Steel Institute (1971) 101-106.

[53] J.J. Jonas, X. Quelennec, L. Jiang, É. Martin, The Avrami kinetics of dynamic recrystallization, Acta Mater. 57 (2009) 2748-2756.

[54] H. Zhao, E.J. Palmiere, Effect of Austenite Deformation on the Microstructure Evolution and Grain Refinement Under Accelerated Cooling Conditions, Metall. Mater. Trans. A 48 (2017) 3389-3399.

[55] J.J. Jonas, Transformation textures associated with steel processing, Microstructure and Texture in Steels, Springer2009, pp. 3-17.

[56] J. Rasti, A. Najafizadeh, M. Meratian, Influence of grain size on the dynamic recrystallization behavior of AISI 304 stainless steel during hot deformation, Int. J. Mater. Res. 103 (2012) 483-489.

[57] A. Dehghan-Manshadi, P. Hodgson, Dependency of recrystallization mechanism to the initial grain size, Metall. Mater. Trans. A 39 (2008) 2830-2840.

[58] H. Kitahara, R. Ueji, N. Tsuji, Y. Minamino, Crystallographic features of lath martensite in low-carbon steel, Acta Mater. 54 (2006) 1279-1288.

[59] S. Kim, Y. Kim, Y. Lim, N.J. Kim, Relationship between yield ratio and the material constants of the Swift equation, Metals and Materials International 12 (2006) 131-135.

[60] G. Speich, L. Cuddy, C. Gordon, A. DeArdo, Formation of ferrite from control-rolled austenite, Phase transformations in ferrous alloys (1983) 341-389.